Article:
Braitor, A.-C., Konstantopoulos, G. and Kadirkamanathan, V. (2021) Current-limiting droop control design and stability analysis for paralleled boost converters in DC micro-grids. IEEE Transactions on Control Systems Technology, 29 (1). pp. 385-394. ISSN: 1063-6536

https://doi.org/10.1109/TCST.2019.2951092

Current-limiting droop control design and stability analysis for paralleled boost converters in DC micro-grids

A.-C. Braitor, *Student Member, IEEE,* G. C. Konstantopoulos, *Member, IEEE,* and V. Kadirkamanathan, *Member, IEEE*

***Abstract*—In this paper, a novel current-limiting droop controller for paralleled DC/DC boost converters loaded by constant impedance Z, constant current I or constant power P loads in a DC micro-grid is proposed to guarantee closed-loop stability and power sharing. Using an improved version of the recently proposed nonlinear current-limiting controller, an inherent current-limiting property is guaranteed for each converter independently from the load type or magnitude variations. Then, sufficient conditions to ensure closed-loop stability for the entire DC micro-grid system with constant Z, I or P loads are analytically obtained. Hence, compared to existing droop control methodologies, the proposed controller ensures accurate power sharing, tight voltage regulation and closed-loop stability with a current limitation when connected to Z, I or P loads, for multiple paralleled boost converters, which introduce nonlinear dynamics. To verify the effectiveness of the proposed controller and the stability analysis, simulation results for three parallel operated DC/DC boost converters with Z, I and P loads and experimental results for two parallel operated DC/DC boost converters with a P load are performed under several changes of the load power demand.**

***Index Terms*—DC micro-grids, droop control, constant power load, stability, current-limiting property.**

I. Introduction

DC micro-grids have gained increased interest in modern power systems since several distributed energy resources, such as photovoltaic systems, fuel cells and battery storage systems run on DC power [1]. Compared to AC micro-grids, DC micro-grids lead to higher efficiency, simpler control design and increased resilience and robustness. As a consequence, DC frameworks have started to be widely employed in electric vehicles, aircraft and shipboard power systems [2], [3], [4].

In these DC frameworks, distributed generation (DG) units are usually connected to a common DC bus through DC/DC converters feeding various types of loads. Such DC/DC power converters operate in parallel and the main challenge is to share the load in proportion to their power ratings. A common practice to accomplish this without overloading some of the sources and without communication is to introduce a virtual resistance at the output of each converter, a technique known as droop control [5], [6], [7]. However, this strategy suffers from significant terminal voltage drop and cannot guarantee accurate power sharing. In [8], a robust droop control method has been proposed to address these drawbacks, where the line impedances are treated as part of the equivalent output impedance of every individual power converter, thus minimizing the inaccuracy in load sharing.

This work is supported by EPSRC under Grants No EP/S001107/1 and EP/S031863/1. The authors are with the Department of Automatic Control and Systems Engineering, The University of Sheffield, Sheffield, S1 3JD, UK, {abraitor1,g.konstantopoulos,visakan}@sheffield.ac.uk.

While droop control has been widely applied in DC micro-grids, the stability of parallel operated DC/DC converters has not been adequately addressed. The main reason rests in the complexity of the DC micro-grid dynamics that increases due to the nonlinear characteristics of the DC/DC converters and their loads. A generic nonlinear model for the loads has already been adopted in [9], called "ZIP", and includes constant impedance Z, constant current I, and constant power P loads; the latter being also the most common and most challenging to deal with due to its well-known negative impedance characteristic, which can lead to instability in DC micro-grids. This destabilizing effect is referred to as 'negative impedance instability' [10]. Thus, there is an increased interest in designing droop controllers that guarantee closed-loop system stability for DC micro-grids loaded by P loads [11], [12], [13], [14].

The majority of the existing stability methods for investigating DC micro-grids are based on the small-signal model of the power devices and linearization approaches, mostly using the Middlebrook and Cuk criterion [15]. Although small-signal modeling is useful to obtain the system's open-loop gain by considering only the input impedance of the loads and output impedance of the sources [16], [17], the stability results that are often obtained, are based on the parameters of a given case study and cannot be generalized. In addition to the theoretic stability proof of the micro-grid, other control issues that relate to the technical requirements of each DG unit should be taken into account in the control design such as the capability of the power converters to be protected at all times, particularly during transients, faults and unrealistic power demands. In this framework, the current-limiting property as outlined in [18], [19], guarantees the converter operation and protection of the equipment without violating certain bounds, as imposed by the technical requirements of each device. Despite the existing strategies that are based on protection units such as using additional fuses, circuit breakers or relays [20], [21], the challenge still rests on designing control methods that can ensure an inherent current-limiting property [22], [23], [24]. Although current-limiting control methods based on saturated PI controllers are often used to guarantee a given upper limit for the current, the main drawbacks of these methods are: i) only the reference value of the converter's current is limited, i.e. the current-limiting property does not hold during transients [19] and ii) closed loop stability cannot be analytically guaranteed since the controller can suffer from integrator windup problems that can potentially lead to instability [25].

To this end, in this paper, a new nonlinear droop controller

is proposed for parallel operated DC-DC boost converters feeding a Z, I or P load in a DC micro-grid architecture in order to ensure accurate power sharing among the paralleled units in proportion to their power ratings and inherent current limitation. Based on the nonlinear dynamics introduced by the boost converters and inspired by the recently proposed current-limiting control [19], an improved current-limiting droop control structure is obtained to guarantee an inherent current-limiting property for each converter independently from each other or the load, accurate power sharing and tight load voltage regulation close to the rated value. Furthermore, the stability of the closed-loop system with n paralleled DC/DC boost converters is proven when connected to a Z, I or P load using singular perturbation theory. The effectiveness of the proposed controller is verified through simulation and experimental testing, and the latter is compared to the cascaded PI technique to highlight its superiority.

It is underlined that compared to the cascaded PI approach or methods that guarantee stability only for a linear resistive load [26], [19], in this paper a new control structure is proposed that inherently limits each converter's current and additionally guarantees closed-loop system stability with Z, I or P loads. In addition, in contrast to the conventional control methods and the stability analysis of the DC micro-grid presented in [13], the novel contribution of the proposed work is highlighted by the following aspects: i) the parallel operation of DC/DC boost converters is investigated here, which are inherently nonlinear systems, opposed to the buck converters studied in [13] which have linear dynamics, ii) improved power sharing and closer voltage regulation to the rated value are achieved by the proposed controller, iii) an inherent current limitation is introduced via the proposed control design for all power converters and iv) conditions for closed-loop stability have been derived for different types of loads (Z, I or P loads). Therefore, according to the authors' knowledge, this is the first time that closed-loop system stability of a DC micro-grid with Z, I or P loads is proven using multiple DC/DC boost converters, which have nonlinear dynamics, while the proposed controller guarantees accurate power sharing, voltage regulation close to the rated value and an inherent current-limiting property.

II. Dynamic Model of a DC Micro-Grid

A. Notation

Given a n-dimensional vector $x{=}[x_1...x_n]$, let $[x]{\in}\mathbb{R}^{n\times n}$ be defined as the diagonal matrix whose diagonal entries are the elements of vector x. Let $\mathbf{0}_n$ be the square matrix with all elements zero, I_n be the identity matrix, $\mathbf{1}_n{\in}\mathbb{R}^n$ and $\mathbf{1}_{n\times n}{\in}\mathbb{R}^{n\times n}$ be the vector and matrix, with all elements equal to one, respectively.

B. Dynamic Model

Fig. 1 shows the configuration of a DC micro-grid consisting of n DC/DC boost converters connected in parallel and feeding a common load. Each converter consists of a boosting inductor L_i, a smoothing capacitor C_i, while U_i is the DC input voltage and R_i the output resistance, where $i \in \{1, 2, ..., n\}$. In [27] the impact of cable impedance on system stability is analyzed, where it is shown that the inductance has no effect on the system stability; hence, for simplicity the cable impedance is regarded as purely resistive.

Using Kirchhoff laws and average analysis [28], the nonlinear dynamic model of each DC/DC boost converter, can be described by the following differential equations:

$$L_i\dot{i}_{Li} = U_i - (1-u_i)V_i \quad (1)$$
$$C_i\dot{V}_i = (1-u_i)i_{Li} - i_i \quad (2)$$

where u_i is the duty-ratio input, which by definition should remain bounded in the range $[0, 1]$, i_{Li} is the inductor current and V_i, i_i are the converter output voltage and current, respectively.

Rewriting (1)-(2) in a matrix form, the DC micro-grid system takes the following form

$$\dot{i}_L = L^{-1}\left(U - (I_n - u)V\right) \quad (3)$$
$$\dot{V} = C^{-1}\left((I_n - u)i_L - i\right) \quad (4)$$

where $U{=}[U_1...U_n]^T$, $u{=}diag\{u_i\}$, $V{=}[V_1...V_n]^T$, $i_L{=}[i_{L1}...i_{Ln}]^T$, $i{=}[i_1...i_n]^T$, $L{=}diag\{L_i\}$ and $C{=}diag\{C_i\}$.

One can observe that system (3)-(4) is nonlinear, since the control input u is multiplied with the system states, $\left[\begin{array}{cc} i_L^T & V^T \end{array}\right]^T$.

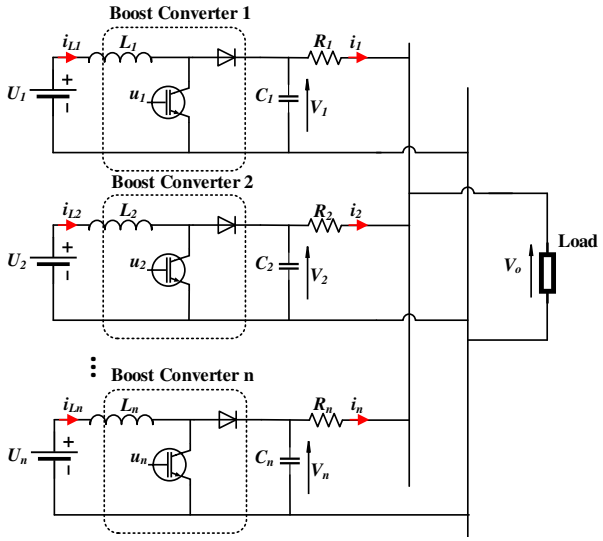

Figure 1. DC micro-grid configuration with n paralleled DC/DC boost converters feeding a common load

One can notice, that the output currents have the following expression $i_i = \frac{V_i - V_o}{R_i}$. Thus, the load voltage can be derived as follows depending on the load type:

1) constant impedance (Z) load: The characteristic equation can be written as

$$\sum_{i=1}^{n} \frac{V_i - V_o}{R_i} = V_o G, \quad (5)$$

where $\frac{1}{G}$ is constant and represents the load resistance. From (5), the load voltage becomes

$$V_o = \frac{\sum_{i=1}^{n} \frac{V_i}{R_i}}{G + \sum_{i=1}^{n} \frac{1}{R_i}}. \quad (6)$$

2) constant current (I) load: In this case the characteristic equation is

$$\sum_{i=1}^{n} \frac{V_i - V_o}{R_i} = i_{load}, \quad (7)$$

where i_{load} is constant and represents the load current. The expression of the load voltage becomes

$$V_o = \frac{\sum_{i=1}^{n} \frac{V_i}{R_i} - i_{load}}{\sum_{i=1}^{n} \frac{1}{R_i}}. \tag{8}$$

3) constant power (P) load: The power balance equation yields

$$V_o \sum_{i=1}^{n} \frac{V_i - V_o}{R_i} = P, \tag{9}$$

where P is constant and represents the power of the P load. Consider now the following assumption:

Assumption 1 *For $\forall\, i = 1, 2...n$, it holds that*

$$\left(\sum_{i=1}^{n} \frac{V_i}{R_i} \right)^2 > 4P \sum_{i=1}^{n} \frac{1}{R_i}.$$

Thus, the expression for the load voltage is given by the real solutions of the second order polynomial

$$V_o = \frac{\sum_{i=1}^{n} \frac{V_i}{R_i} \pm \sqrt{\left(\sum_{i=1}^{n} \frac{V_i}{R_i} \right)^2 - 4P \sum_{i=1}^{n} \frac{1}{R_i}}}{2 \sum_{i=1}^{n} \frac{1}{R_i}}. \tag{10}$$

Assumption 2 *For $\forall\, i = 1, 2...n$, there is $V_i \geq U_i$, which represents a requirement for any DC/DC boost converter.*

Please note that based on Assumption 1 and 2, solution (10) exists if $\left(\sum_{i=1}^{n} \frac{U_i}{R_i} \right)^2 > 4P \sum_{i=1}^{n} \frac{1}{R_i}$.

Assumption 3 *Let Assumption 2 hold. If $i_{Li}^{max} > 0$ represents the maximum inductor current of each converter, i.e. $|\, i_{Li}\,| < i_{Li}^{max}$, let $U_i - i_{Li}^{max} R_i > \frac{\sum_{i=1}^{n} \frac{V_i}{R_i} - \sqrt{\left(\sum_{i=1}^{n} \frac{V_i}{R_i} \right)^2 - 4P \sum_{i=1}^{n} \frac{1}{R_i}}}{2 \sum_{i=1}^{n} \frac{1}{R_i}}$ hold.*

The load voltage (10) has two solutions, a high voltage and a low voltage, with the high voltage representing the feasible solution because of *Assumption 2 and 3, which yield* $V_o \geq U_i - i_{Li}^{max} R_i$, a fact also considered in [29]. Therefore

$$V_o = \frac{\sum_{i=1}^{n} \frac{V_i}{R_i} + \sqrt{\left(\sum_{i=1}^{n} \frac{V_i}{R_i} \right)^2 - 4P \sum_{i=1}^{n} \frac{1}{R_i}}}{2 \sum_{i=1}^{n} \frac{1}{R_i}}. \tag{11}$$

Hence, a generalized expression for the load voltage in all three cases can be found as

$$V_o = \frac{\sum_{i=1}^{n} \frac{V_i}{R_i} + \alpha}{\beta + \sum_{i=1}^{n} \frac{1}{R_i}}. \tag{12}$$

where α and β have the expressions specified in Table I.

Table I

	Z	I	P
α	0	$-i_{load}$	$\sqrt{\left(\sum_{i=1}^{n} \frac{V_i}{R_i} \right)^2 - 4P \sum_{i=1}^{n} \frac{1}{R_i}}$
β	G	0	$\sum_{i=1}^{n} \frac{1}{R_i}$

III. Proposed Controller Design

The aim of the control design is to achieve power sharing among the paralleled converters and tight load voltage regulation close to the rated value, while maintaining a limited input current for each converter. Here the droop control concept is implemented as a dynamic virtual resistance for each converter, opposed to the traditional design, which is applied directly to the voltage. Hence, the duty-ratio input of each boost converter takes the form

$$u_i = 1 - \frac{w_i}{V_i} i_{Li}, \tag{13}$$

where $i \in \{1, 2, \ldots, n\}$ indicates the converter number and w_i represents a virtual resistance for i-th converter. Inspired by the current-limiting controller [19], the virtual resistance is proposed to follow the nonlinear dynamics:

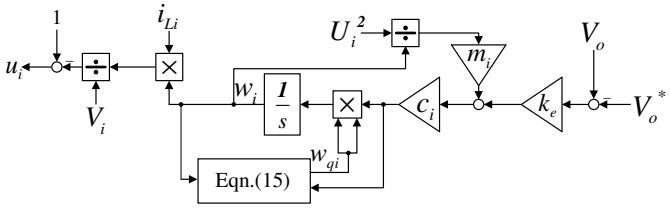

Figure 2. Implementation diagram of the proposed controller

$$\dot{w}_i = -c_i w_{qi}^2 \left[k_e (V_o^* - V_o) - m_i \frac{U_i^2}{w_i} \right] \tag{14}$$

$$\dot{w}_{qi} = c_i \frac{(w_i - w_{mi})}{\Delta w_{mi}^2} w_{qi} \left[k_e (V_o^* - V_o) - m_i \frac{U_i^2}{w_i} \right] - c_i k_{qi} \left(\frac{(w_i - w_{mi})^2}{\triangle w_{mi}^2} + w_{qi}^2 - 1 \right) w_{qi}, \tag{15}$$

with c_i, k_{qi}, k_e, w_{mi}, $\triangle w_{mi}$ being positive constants and V_o^*, m_i representing the load voltage reference and the droop coefficient, respectively. In contrast to the robust droop controller [8], the proposed controller does not require the measurement of the output current i_i of each converter; thus leading to a simpler implementation and also facilitating the stability analysis in Section IV. It is highlighted that the proposed structure of the control dynamics guarantees a given bound for w_i based on the bounded integral controller concept [30]. For more details on the boundedness of w_i and w_{qi} the reader is referred to [30] where it is shown that $w_i \in [w_i^{min}, w_i^{max}] > 0$ and $w_{qi} \in [0, 1]$ for all $t \geq 0$, given typical initial conditions $w_{i0} = w_{mi}$ and $w_{qi0} = 1$. Note also that due to the current-limiting property of the proposed controller, given $i_{Li}^{max} > 0$, then if $w_i^{min} = w_{mi} - \triangle w_{mi} = \frac{U_i}{i_{Li}^{max}}$, then $|\, i_{Li}(t)\,| \leq i_{Li}^{max}$, $\forall t \geq 0$ (see [19]). A control diagram with the controller and all sensed feedback variables is shown in Fig. 2.

Assumption 4 *For every constant $w_{ie} \in \left(w_i^{min}, w_i^{max} \right) > 0$, satisfying*

$$m_1 \frac{U_1^2}{w_{1e}} = m_2 \frac{U_2^2}{w_{2e}} = ... = m_n \frac{U_n^2}{w_{ne}}. \tag{16}$$

there exists a unique steady-state equilibrium point $(i_{Lie}, V_{ie}, w_{ie}, w_{qie})$ corresponding to the desired voltage regulation, i.e.

$$V_{oe} = V_o^* - \frac{m_i U_i^2}{k_e w_{ie}} \tag{17}$$

where $w_{qie} \in (0, 1]$, $\forall i = 1, 2...n$.

Assumption 5 *For $\forall i = 1, 2...n$, it holds that $\frac{k_e}{m_i V_{ie}} - \frac{1}{R_i} > 0$.*

By replacing the expression of the proposed controller (13) into the inductor current equation (1), the closed-loop dynamics of the inductor current for each converter become:

$$L_i \dot{i}_{Li} = -w_i i_{Li} + U_i, \tag{18}$$

where it is clear that w_i represents a virtual resistance in series with the inductance L_i. The equivalent closed-loop system is given in Fig. 3, where it is clear that the current i_{Li} dynamics of each converter are partially decoupled from the voltages V_i. At the steady-state there is

$$i_{Lie} = \frac{U_i}{w_{ie}}. \tag{19}$$

Hence, the term $\frac{U_i^2}{w_i}$ represents the input power of each converter at the steady-state. As a result, (16) yields

$$m_1 P_1 = m_2 P_2 = ... = m_n P_n$$

which indicates the desired power sharing in the DC micro-

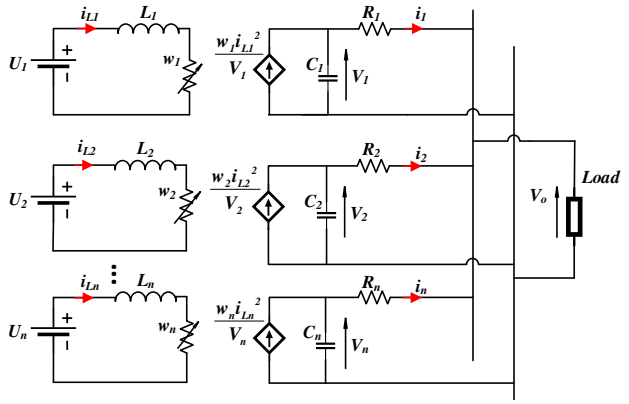

Figure 3. Equivalent circuit of the closed-loop system

grid based on a suitable choice of the droop parameters m_i.

IV. Stability Analysis

A. Closed-loop system

By applying the proposed controller (13)-(15) into the DC micro-grid dynamics (1)-(2), the closed-loop system can be written in the following matrix form

$$\begin{bmatrix} \dot{i}_L \\ \dot{V} \end{bmatrix} = \begin{bmatrix} L^{-1}\left(U-[w]\,i_L\right) \\ C^{-1}\left([V]^{-1}\,[i_L]^2\,w-i\right) \end{bmatrix} \tag{20}$$

$$\begin{bmatrix} \dot{w} \\ \dot{w}_q \end{bmatrix} = \begin{bmatrix} -c\,[w_q]^2\left(k_e(V_o^*-V_o)\mathbf{1}_n-[U]^2\,[w]^{-1}\,m\right) \\ c([w]-w_m)\triangle w_m^{-2}\,[w_q]\left(k_e(V_o^*-V_o)\mathbf{1}_n-[U]^2\,[w]^{-1}m\right) \\ -ck_q\left(([w]-w_m)^2\triangle w_m^{-2}+[w_q]^2-I_n\right)w_q \end{bmatrix} \tag{21}$$

where $w=[w_1...w_n]^T$, $w_q=[w_{q1}...w_{qn}]^T$, $c=diag\{c_i\}$, $m=[m_1...m_n]^T$, $k_q=diag\{k_{qi}\}$, $w_m=diag\{w_{mi}\}$, $\triangle w_m=diag\{\triangle w_{mi}\}$.

Consider an equilibrium point $(i_{Lie}, V_{ie}, w_{ie}, w_{qie})$ satisfying Assumption 4. By setting $\varepsilon=\frac{1}{min\{c_i\}}$, there exists $\delta=diag\{\delta_i\}\geq 0$ such that $c=\frac{1}{\varepsilon}I_n+\delta$. Hence, (21) becomes

$$\begin{bmatrix} \varepsilon\dot{w} \\ \varepsilon\dot{w}_q \end{bmatrix} = \begin{bmatrix} -\left(I_n+\varepsilon\delta\right)[w_q]^2\left(k_e(V_o^*-V_o)\mathbf{1}_n-[U]^2[w]^{-1}m\right) \\ \left(I_n+\varepsilon\delta\right)([w]-w_m)\triangle w_m^{-2}[w_q]\left(k_e(V_o^*-V_o)\mathbf{1}_n-[U]^2[w]^{-1}m\right) \\ -\left(I_n+\varepsilon\delta\right)k_q\left(([w]-w_m)^2\triangle w_m^{-2}+[w_q]^2-I_n\right)w_q \end{bmatrix} \tag{22}$$

Hence, the closed-loop system equations (20) and (22) can be written as

$$\dot{x} = f(x,z) \tag{23}$$

$$\varepsilon\dot{z} = g(x,z,\varepsilon) \tag{24}$$

where $x=\begin{bmatrix} i_L-i_{Le} \\ V-V_e \end{bmatrix}$ and $z=\begin{bmatrix} w-w_e \\ w_q-w_{qe} \end{bmatrix}$. For arbitrarily large values of the controller gains c_i, then ε is small and therefore (23)-(24) can be investigated as a singularly perturbed system using two-time-scale analysis [31]. The controller's system (22) is also named as the boundary layer since it represents the immediate vicinity of a bounding surface and is first analyzed in the sequel.

B. Boundary layer stability analysis

Considering f, g being continuously differentiable in the domain $(x,z,\varepsilon)\in D_x\times D_z\times[0,\varepsilon_0]$, when the controller gain c is selected sufficiently large, then $\varepsilon\to 0$ and, based on singular perturbation theory, g will have an algebraic form of $0=g(x,z)$ as follows

$$\begin{bmatrix} 0 \\ 0 \end{bmatrix} = \begin{bmatrix} -[w_q]^2\left(k_e(V_o^*-V_o)\mathbf{1}_n-[U]^2[w]^{-1}m\right) \\ ([w]-w_m)\triangle w_m^{-2}\,[w_q]\left(k_e(V_o^*-V_o)\mathbf{1}_n-[U]^2[w]^{-1}m\right) \\ -k_q\left(([w]-w_m)^2\triangle w_m^{-2}+[w_q]^2-I_n\right)w_q \end{bmatrix}. \tag{25}$$

The roots of the above system can be computed as

$$\begin{bmatrix} w \\ w_q \end{bmatrix} = \begin{bmatrix} \frac{1}{k_e(V_o^*-V_o)}\,[U]^2\,m \\ \left(I_n-([w]-w_m)^2\triangle w_m^{-2}\right)^{1/2}\mathbf{1}_n \end{bmatrix} \tag{26}$$

and can also be referred to as $z=h(x)$ with $w_i\in(w_i^{min}, w_i^{max})>0$ and $w_{qi}\in(0,1]$, such that $h(0)=0$. Thus, the roots also represent the equilibrium points of the nonlinear system (20)-(21). Exponential stability at the origin can be investigated via its corresponding Jacobian matrix:

$$J_1=\begin{bmatrix} -[w_{qe}]^2\,[U]^2\,[w_e]^{-2}\,[m] & \mathbf{0}_n \\ -\left([w_e]-w_m\right)\triangle w_m^{-2}\,[w_{qe}]\,[U]^2\,[w_e]^{-2}\,[m] & -2k_q[w_{qe}]^2 \\ -2k_q\left([w_e]-w_m\right)\triangle w_m^{-2}\,[w_{qe}] & \end{bmatrix}$$

One can see that matrix J_1 is Hurwitz, as it is lower triangular and all diagonal elements are negative. Hence, there exist $\rho_1>0$ and a domain $\tilde{D}_z=\{z\,\epsilon\,R^{2n}, \|z\|_2<\rho_1\}$ where $\tilde{D}_z\subseteq D_z$ such that (24) is exponentially stable at the origin uniformly in x.

C. Admittance matrix

Taking the partial derivative of the output current $i_i=\frac{V_i-V_o}{R_i}$ with respect to the output voltage V_i, we get the admittance matrix

$$Y=\frac{\partial i_i}{\partial V_i}=\begin{bmatrix} \frac{1}{R_1}\left(1-\frac{\partial V_o}{\partial V_1}\right) & -\frac{1}{R_1}\frac{\partial V_o}{\partial V_2} & \cdots & -\frac{1}{R_1}\frac{\partial V_o}{\partial V_n} \\ -\frac{1}{R_2}\frac{\partial V_o}{\partial V_1} & \frac{1}{R_2}\left(1-\frac{\partial V_o}{\partial V_2}\right) & \cdots & -\frac{1}{R_2}\frac{\partial V_o}{\partial V_n} \\ \vdots & \vdots & \ddots & \vdots \\ -\frac{1}{R_n}\frac{\partial V_o}{\partial V_1} & -\frac{1}{R_n}\frac{\partial V_o}{\partial V_2} & & \frac{1}{R_n}\left(1-\frac{\partial V_o}{\partial V_n}\right) \end{bmatrix}$$

$$=R^{-1}\left(I_n-\begin{bmatrix} 1\ldots 1 \\ \vdots\ \ddots\ \vdots \\ 1\ldots 1 \end{bmatrix}\begin{bmatrix} \frac{\partial V_o}{\partial V_1}\ \cdots\ 0 \\ \vdots\ \ddots\ \vdots \\ 0\ \ldots\ \frac{\partial V_o}{\partial V_n} \end{bmatrix}\right)=R^{-1}(I_n-\mathbf{1}_{n\times n}D) \tag{27}$$

where $R=diag\{R_i\}$, and

$$D=diag\left\{\frac{\partial V_o}{\partial V_i}\right\}=\frac{1}{\beta+\sum_{i=1}^n\frac{1}{R_i}}\left(R^{-1}+\begin{bmatrix} \frac{\partial\alpha}{\partial V_1}\ \cdots\ 0 \\ \vdots\ \ddots\ \vdots \\ 0\ \ldots\ \frac{\partial\alpha}{\partial V_n} \end{bmatrix}\right) \tag{28}$$

with $\beta\geq 0$. Please note that for the Z and I load cases, there is $\begin{bmatrix} \frac{\partial\alpha}{\partial V_1}\ \cdots\ 0 \\ \vdots\ \ddots\ \vdots \\ 0\ \ldots\ \frac{\partial\alpha}{\partial V_n} \end{bmatrix}=\mathbf{0}_n$, while for the P load case, it becomes

$$\begin{bmatrix} \frac{\partial\alpha}{\partial V_1}\ \cdots\ 0 \\ \vdots\ \ddots\ \vdots \\ 0\ \ldots\ \frac{\partial\alpha}{\partial V_n} \end{bmatrix}=\frac{\sum_{i=1}^n\frac{V_{ie}}{R_i}}{\sqrt{\left(\sum_{i=1}^n\frac{V_{ie}}{R_i}\right)^2-4P\sum_{i=1}^n\frac{1}{R_i}}}\begin{bmatrix} \frac{1}{R_1}\ \cdots\ 0 \\ \vdots\ \ddots\ \vdots \\ 0\ \ldots\ \frac{1}{R_n} \end{bmatrix}$$

$$=\frac{\sum_{i=1}^n\frac{V_{ie}}{R_i}}{\alpha_e}R^{-1}$$

where α_e is given from Table I with $V_i=V_{ie}$. It is clear that in all three load cases (Z, I and P), matrix D is a positive-definite diagonal matrix.

D. Reduced model

To obtain the reduced model, the roots w and w_q are substituted from (26) into (20), yielding

$$\dot{i}_L = L^{-1}\left(U-\frac{1}{k_e(V_o^*-V_o)}\,[U]^2\,[m]\,i_L\right) \tag{29}$$

$$\dot{V} = C^{-1}\left(\frac{1}{k_e(V_o^*-V_o)}\,[U]^2\,[V]^{-1}\,[i_L]^2\,m-i\right). \tag{30}$$

This model is often referred to as quasi-steady-state model, because w, w_q introduce a velocity $[\dot{w}\ \dot{w}_q]^T = \varepsilon^{-1} g$ which is very large when ε is small and $g \neq 0$, leading to rapid convergence to a root $h(i_L, V)$, which is the equilibrium of the boundary-layer. The corresponding Jacobian matrix of the reduced system will have the following form

$$J_2 = \begin{bmatrix} \frac{1}{k_e(V_o^* - V_{oe})} L^{-1}[U]^2[m] & -\frac{1}{V_o^* - V_{oe}} L^{-1}[U]\mathbf{1}_{n\times n} D \\ 2C^{-1}[U][V_e]^{-1} & C^{-1}\left(k_e[V_e]^{-1}[m]^{-1}\left(\mathbf{1}_{n\times n} D - (V_o^* - V_{oe})[V_e]^{-1}\right) - Y\right) \end{bmatrix}$$

The characteristic equation can be calculated from

$$|\lambda I_n - J_2| = |\lambda^2 I_n + \lambda M + N| = 0, \tag{31}$$

with

$$M = \frac{1}{k_e(V_o^* - V_{oe})} L^{-1}[U]^2[m] - C^{-1}\left(k_e[V_e]^{-1}[m]^{-1}\left(\mathbf{1}_{n\times n} D - (V_o^* - V_{oe})[V_e]^{-1}\right) - Y\right) \tag{32}$$

$$N = \frac{1}{k_e(V_o^* - V_{oe})} L^{-1}[U]^2[m] C^{-1}\left(k_e[V_e]^{-1}[m]^{-1}\left((V_o^* - V_{oe})[V_e]^{-1} + \mathbf{1}_{n\times n} D\right) + Y\right) \tag{33}$$

Replacing matrix Y with its expressions from (27), and isolating matrix $\mathbf{1}_{n\times n}$ by factorization, followed by left and right multiplication with determinants $|D| > 0$ and $|X| = \frac{1}{k_e(V_o^* - V_{oe})} |L^{-1}[U]^2[m] C^{-1}\left(k_e[V_e]^{-1}[m]^{-1} - R^{-1}\right)| > 0$, according to Assumption 5, respectively, the characteristic polynomial becomes

$$|\lambda^2 X^{-1} D^{-1} + \lambda \overline{M} + \overline{N}| = 0, \tag{34}$$

which is a quadratic eigenvalue problem (QEP) with $\overline{N}$ symmetrical and $\overline{M}$, according to Lemma 2 in [13], diagonalizable whose eigenvalues are all real, since it is a product between a positive-definite diagonal and a symmetrical matrix. Since $\overline{M} = P^{-1}\Lambda P$, equation (34) can be rewritten as

$$|\lambda^2 P X^{-1} D^{-1} P^{-1} + \lambda\Lambda + P\overline{N}P^{-1}| = 0, \tag{35}$$

with Λ being a diagonal matrix with the eigenvalues of matrix $\overline{M}$ as main entries. The similarity transformation $PX^{-1}D^{-1}P^{-1}$ and $P\overline{N}P^{-1}$ are symmetrical, as P is an orthogonal matrix, i.e. $P^{-1} = P^T$, and they share the same eigenvalues as $X^{-1}D^{-1} > 0$ and $\overline{N}$, respectively. If $\Lambda > 0$, or equivalently $\overline{M}$ has positive eigenvalues, and $\overline{N} > 0$, then $Re(\lambda) < 0$ and J_2 is Hurwitz. Since matrix $\overline{M}$ is represented by a multiplication where one term is the diagonal matrix $X^{-1}\left(C^{-1}k_e[V_e]^{-1}[m]^{-1} + C^{-1}R^{-1}\right) > 0$, according to Sylvester's law on inertia, matrix $\overline{M}$ will have the same index of inertia as the remaining term, $\left(C^{-1}k_e[V_e]^{-1}[m]^{-1} + C^{-1}R^{-1}\right)^{-1}\overline{M}$. According to Lemma 1 in [13], if

$$\frac{U_i^2 m_i}{k_e(V_o^* - V_{oe})L_i} + \frac{1}{C_i}\left(\frac{k_e}{m_i V_{ie}}\left(\frac{V_o^* - V_{oe}}{V_{ie}} - \lambda_{Di} n\right) + \frac{1}{R_i}(1 - \lambda_{Di} n)\right) > 0,\ \forall i = 1...n, \tag{36}$$

holds, then $\overline{M} > 0$ is satisfied. For the Z and I load cases, all eigenvalues of matrix D are $\lambda_{Di} = \frac{1}{\beta + \sum_{i=1}^{n} \frac{1}{R_i}} \frac{1}{R_i} > 0$, while for the P load case, there is $\lambda_{Di} = \frac{1}{\beta + \sum_{i=1}^{n} \frac{1}{R_i}} \frac{1}{R_i}\left(1 + \frac{\sum_{i=1}^{n} \frac{V_{ie}}{R_i}}{\alpha_e}\right) > 0$.

Regarding condition $\overline{N} > 0$, by considering Assumption 5, if

$$\frac{k_e}{m_i V_{ie}}\left(\frac{V_o^* - V_{oe}}{V_{ie}\lambda_{Di}} + n\right) + \frac{1}{R_i}\left(\frac{1}{\lambda_{Di}} - n\right) > 0,\ \forall i = 1...n. \tag{37}$$

holds, then $\overline{N} > 0$ is satisfied. Hence, if the two conditions (36)-(37) hold for each converter then there exist $\rho_2 > 0$ and a domain $\tilde{D}_x = \{x \in R^{2n}, \|x\|_2 < \rho_2\}$ where $\tilde{D}_x \subseteq D_x$ such that the reduced model is exponentially stable at the origin.

According to *Theorem* 11.4 in [31], there exists ε^* such that for all $\varepsilon < \varepsilon^*$, the equilibrium point $[i_{Le}^T\ V_e^T\ w_e^T\ w_{qe}^T]^T$ of (20)-(22) with $w_{ie} \in (w_i^{min}, w_i^{max})$ and $w_{qie} \in (0, 1]$ is exponentially stable; thus completing the stability analysis of the entire DC micro-grid. Note that the stability conditions (36)-(37) can also provide a useful guidance for the converter or micro-grid design (eg. selection of values for C_i, L_i, R_i, etc.).

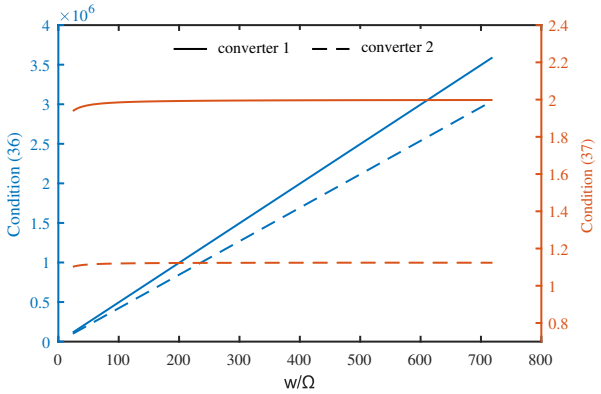

Figure 4. Checking stability conditions (36)-(37)

V. Methodology for Testing the Stability Conditions

Conditions (36)-(37) might initially seem difficult to verify, mainly because they require the calculation of the equilibrium point, which, in a micro-grid, is a daunting task [13], [32]. However due to the particular design of the proposed current-limiting droop controller and the boundedness properties of w_i and w_{qi}, the following pseudo-code written procedure can be used to test the conditions, for the P load case as an example:

%Test for any w_{1e} in the range (w_1^{min}, w_1^{min})

For $w_{1e} = w_{1e}^{min} + \delta$ *to* $w_1^{max} - \delta$
Calculate w_{je} *from* (16) *for all* $j = 2, ..., n$
if $w_j^{min} < w_{je} < w_j^{max}$ *for all* $j = 2, ..., n$
Calculate i_{Li}^e *from* (19);
Calculate V_o^e *from* (17);
Calculate $V_e = diag\{V_{ie}\}$ *by combining* (4), (17), (19) and the power P using (9);
Calculate α *and* β *from Table I and the diagonal elements of* D from (28);
%Check stability conditions
Check conditions (36)-(37);
end;
end.

In order to verify this methodology, the practical example that will be tested in Section VII is investigated. The system represents a DC micro-grid with two boost converters in parallel feeding a P load, where each unit is equipped with the proposed controller based on the parameters specified in Table III. The results of the two stability conditions are shown in Fig. 4, where it is clear that for any w_1 in the bounded range (w_1^{min}, w_1^{max}), the expressions (36)-(37) for each converter are positive, thus guaranteeing closed-loop system stability.

VI. Simulation Results

To verify the aforementioned analysis, a DC micro-grid with the parameters given in Table II, consisting of three boost converters feeding a common load is simulated for $20s$. The main tasks are to regulate the load voltage close to $400V$, share the power in a $3:2:1$ ratio, and maintain an upper bound for the input current, when different types of loads (Z, I and P) are connected at the common bus.

During the first 5 seconds, the three converters are feeding a common Z load with a load resistance $\frac{1}{G} = 400\Omega$. It can

be observed in Fig. 5a that the currents are accurately shared in a $3:2:1$ ratio, having $i_1 = 0.5A$, $i_2 = 0.33A$, $i_3 = 0.166A$, provided the input currents haven't reached their imposed limit yet (Fig. 5b). The load voltage is regulated close to the rated value as seen in Fig. 5c where $V_o = 399V$.

Table II
CONTROLLER AND SYSTEM PARAMETERS

Parameters	Values	Parameters	Values
R_1	2.1Ω	U_1	$200V$
R_2	1.9Ω	U_2	$100V$
R_3	1.7Ω	U_3	$240V$
L_1	$2.2mH$	k_e	10
L_2	$2.1mH$	m_1	0.05
L_3	$2.3mH$	m_2	0.075
C_1, C_2, C_3	$560\mu F$	m_3	0.15
i_{L1}^{max}	$2A$	k_{q1}, k_{q2}, k_{q3}	1
i_{L2}^{max}	$5A$	c_1, c_2, c_3	1.26×10^4
i_{L3}^{max}	$2.5A$	i_{L1}^{min}, i_{L2}^{min}, i_{L3}^{min}	$1mA$

At $t = 5s$, the load changes to a constant I load with a load current $i_{load} = 1.5A$. The inductor currents are still below their limit (Fig. 5b), and the output currents (Fig. 5a) keep their accurate sharing $(3:2:1)$ with $i_1 = 0.75A$, $i_2 = 0.5A$, $i_3 = 0.25A$ and the load voltage remains close to $400V$, as one can observe in Fig. 5c where $V_o = 398.5V$.

The load changes to a constant P load at $t = 10s$, with a load power $P = 360W$. From Fig. 5c, it can be seen that the load voltage is $V_o = 399.2V$, while the output currents (Fig. 5a) are $i_1 = 0.45A$, $i_2 = 0.3A$, $i_3 = 0.15A$.

To test the current limitation, at $t = 15s$, the constant P load becomes $P = 840W$. The load voltage drops down to $397.7V$ (Fig. 5c), and the $2:1$ power sharing is kept between converters 2 and 3, with $i_2 = 0.74A$ and $i_3 = 0.37A$ since their input currents have not reached their limit yet. However, for the first converter, the inductor current i_{L1} is successfully limited at its given upper value $i_{L1} = i_{L1}^{max} = 2A$.

VII. EXPERIMENTAL RESULTS

A DC micro-grid with the parameters given in Table III, consisting of two parallel Texas Instruments DC-DC boost converters loaded by a ETPS ELP-3362F electronic load acting as a P load as shown in Fig. 6, is tested to experimentally evaluate the proposed control framework. A switching frequency of $60kHz$ is used for the pulse-width modulation of both converters. The main task is to achieve load voltage regulation close to the rated value V_o^*=$48V$ and accurate power sharing among paralleled converters, while maintaining the inductor currents below their maximum values independently from the

Table III
CONTROLLER AND SYSTEM PARAMETERS

Parameters	Values	Parameters	Values
R_1	2.4Ω	U_1	$36V$
R_2	3Ω	U_2	$24V$
L_1, L_2	$0.3mH$	k_{q1}, k_{q2}	1
C_1, C_2	$300\mu F$	k_e	10
m_1	0.2	i_{L1}^{max}	$1.5A$
m_2	0.4	i_{L2}^{max}	$2.5A$
c_1	1012	i_{L1}^{min}	$50mA$
c_2	517	i_{L2}^{min}	$50mA$

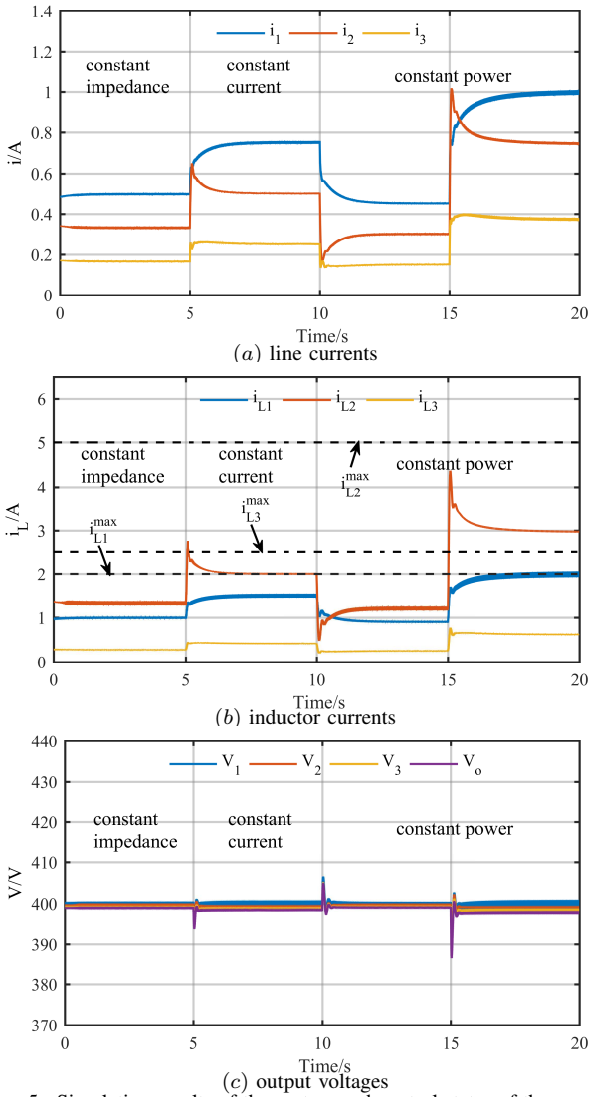

Figure 5. Simulation results of the system and control states of three parallel operated DC-DC boost converters feeding a Z, I and P load

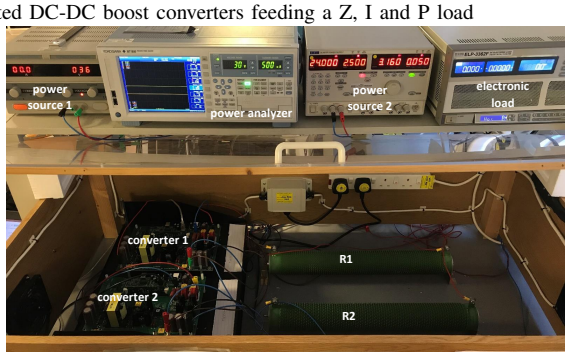

Figure 6. Experimental setup

load changes. In this study, the power of the two sources satisfy the relation P_1=$2P_2$ and, hence, the load should be shared in a 2:1 ratio. To verify the effectiveness of the proposed current-limiting droop controller, it is compared to the cascaded PI approach under the same scenario. The controller parameters were calculated using the following expressions w_{mi}=$\frac{U_i}{2}\left(\frac{1}{i_{Li}^{min}}+\frac{1}{i_{Li}^{max}}\right)$ and Δw_{mi}=$\frac{U_i}{2}\left(\frac{1}{i_{Li}^{min}}-\frac{1}{i_{Li}^{max}}\right)$ as in [19].

Initially, the $40W$ load demand increases to $60W$ and, as one can observe in Fig. 7a, the load is accurately shared using the proposed controller since at steady-state there is i_1=$2i_2$, as i_1≈$0.8A$ and i_2≈$0.4A$, opposed to the case of the conventional

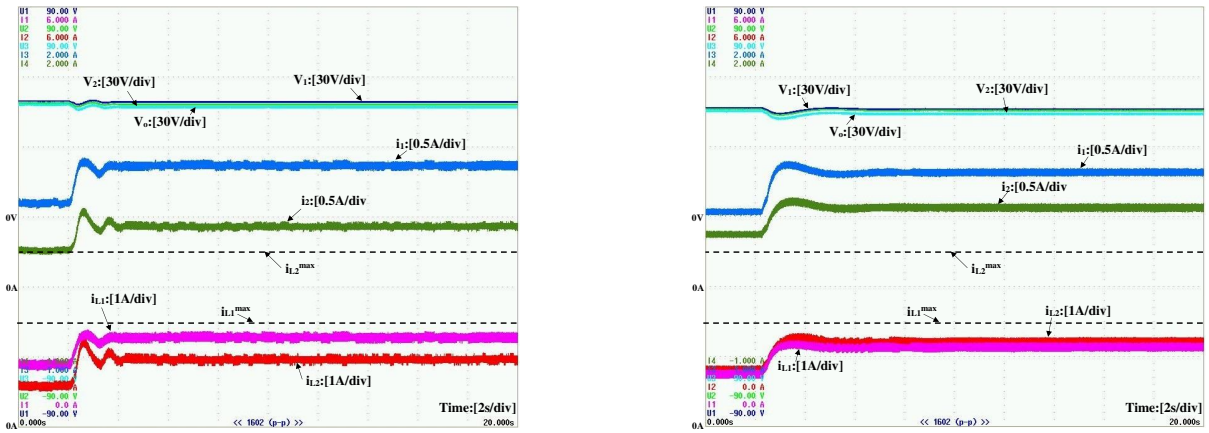

(a) dynamic response when the load demand increases from $40W$ to $60W$

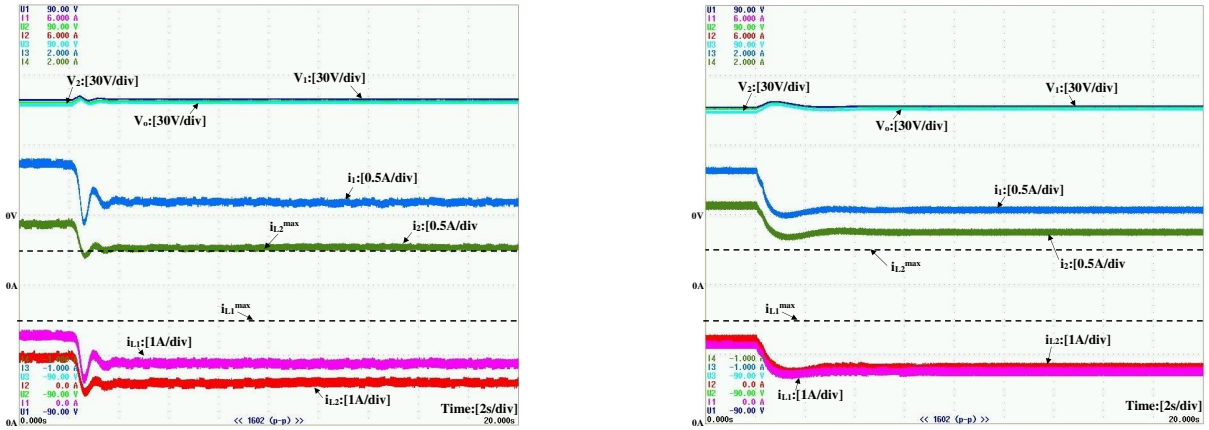

(b) dynamic response when the load demand decreases from $60W$ to $40W$

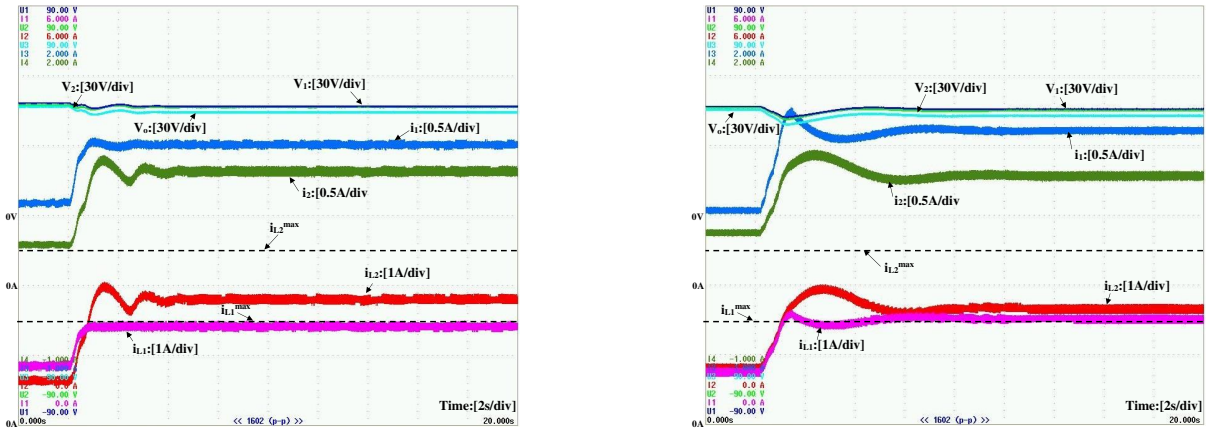

(c) dynamic response when the load demand increases from $40W$ to $80W$

Figure 7. Experimental results of the system states of two parallel operated DC-DC boost converters feeding a P load using the proposed controller (left) and cascaded PI (right)

strategy where $i_1 \neq 2i_2$. The inductor currents remain below their maximum value as imposed by the system parameters. The converters' output voltages are very tightly regulated to the reference, the load voltage remains very close to its rated value (V_{oe}=$47.2V$) using the proposed controller, while for the case of the cascaded PI, it drops by $1.5-2V$.

In Fig. 7b, the load power demand decreases from $60W$ down to $40W$. The power sharing is kept at the 2:1 ratio using the proposed controller having $i_1 \approx 0.6A$ and $i_2 \approx 0.3A$ in contrast to the cascaded PI strategy. The proposed droop control regulates the converters' and load voltages to their new steady-state values after a short transient and V_o still remains closer to the rated value, with V_{oe}=$47.5V$, unlike the cascaded PI framework.

Finally, in Fig. 7c, the load changes from $40W$ to $80W$ in order to test the controller performance under a large P load demand that will require a higher current from converter 1 that exceeds its technical limit. As one can observe, the proposed current-limiting droop controller maintains an upper limit for the inductor current of converter 1 protecting the device, unlike the cascaded PI droop control where the inductor current cannot be limited during transients and also leads to integrator windup. On the other hand, the proposed controller does not require a saturation unit and the current limitation is inherently guaranteed at all times, even during transients. The power sharing is automatically sacrificed by the proposed controller

in order to protect converter 1, which reaches its maximum capacity $i_{L1}{=}i_{L1}^{max}{=}1.5A$. As converter 2 has not violated its own capacity ($i_{L2}{<}i_{L2}^{max}$), the load demand is automatically covered and the voltage of the load is still regulated close to the rated ($V_{oe}{=}46.8V$). This operation is achieved automatically in a decentralized way, verifying the current-limiting property and the stability analysis presented in this paper.

VIII. Conclusions

A new current-limiting droop controller for achieving power sharing among multiple parallel operated DC-DC boost converters in a DC micro-grid architecture, feeding a constant Z, I or P load, was proposed. The proposed controller additionally guarantees an inherent current limitation for each converter independently. The stability of the entire DC micro-grid was analytically proven, while simulation and experimental results were presented to validate the proposed control approach under several changes of the load power demand in comparison to the conventional droop control. The superiority of the proposed current-limiting droop controller with regard to the conventional control is outlined in the following aspects: i) improved power sharing, ii) load voltage regulation closer to the rated value, iii) inherent current-limiting property during transients and iv) proven closed-loop system stability for the nonlinear model of the DC micro-grid with a Z, I or P load.

The main aim of this work was to present for the first time this novel current-limiting droop controller for multiple paralleled boost converters and rigorously guarantee the stability of the system when feeding a Z, I or P load with an inherent current protection embedded in the control design. Future work will focus on improving the transient performance of the controller to reduce undesired oscillations, and combine it with secondary control to restore the load voltage to the rated value in a distributed manner. In addition, it is interesting to investigate how the entire micro-grid stability is affected by delays in the measurements or the control implementation, under different combination of a series-parallel network.

References

[1] Y. Xia, W. Wei, Y. Peng, P. Yang, and M. Yu. Decentralized coordination control for parallel bidirectional power converters in a grid-connected dc microgrid. *IEEE Transactions on Smart Grid*, PP(99):1–1, 2017.

[2] C. Sun, X. Hu, S. J. Moura, and F. Sun. Velocity predictors for predictive energy management in hybrid electric vehicles. *IEEE Transactions on Control Systems Technology*, 23(3):1197–1204, May 2015.

[3] Y. Jia and K. Rajashekara. Induction machine for more electric aircraft: Enabling new electrical power system architectures. *IEEE Electrification Magazine*, 5(4):25–37, Dec 2017.

[4] P. Cairoli and R. A. Dougal. New horizons in dc shipboard power systems: New fault protection strategies are essential to the adoption of dc power systems. *IEEE Electrification Magazine*, 1(2):38–45, Dec 2013.

[5] M. Mahmoodi, G. B. Gharehpetian, M. Abedi, and R. Noroozian. Control systems for independent operation of parallel dg units in dc distribution systems. In *2006 IEEE International Power and Energy Conference*, pages 220–224, Nov 2006.

[6] P. H. Huang, P. C. Liu, W. Xiao, and M. S. El Moursi. A novel droop-based average voltage sharing control strategy for dc microgrids. *IEEE Transactions on Smart Grid*, 6(3):1096–1106, May 2015.

[7] J. Schiffer, T. Seel, J. Raisch, and T. Sezi. Voltage stability and reactive power sharing in inverter-based microgrids with consensus-based distributed voltage control. *IEEE Transactions on Control Systems Technology*, 24(1):96–109, Jan 2016.

[8] Z. Shuai, D. He, J. Fang, Z. J. Shen, C. Tu, and J. Wang. Robust droop control of dc distribution networks. *IET Renewable Power Generation*, 10(6):807–814, 2016.

[9] Claudio De Persis, Erik R.A. Weitenberg, and Florian Dörfler. A power consensus algorithm for dc microgrids. *Automatica*, 89:364 – 375, 2018.

[10] Ali Emadi, Babak Fahimi, and Mehrdad Ehsani. On the concept of negative impedance instability in the more electric aircraft power systems with constant power loads. In *SAE Technical Paper*. SAE International, 08 1999.

[11] H. J. Kim, S. W. Kang, G. S. Seo, P. Jang, and B. H. Cho. Large-signal stability analysis of dc power system with shunt active damper. *IEEE Transactions on Industrial Electronics*, 63(10):6270–6280, Oct 2016.

[12] Q. Xu, C. Zhang, C. Wen, and P. Wang. A novel composite nonlinear controller for stabilization of constant power load in dc microgrid. *IEEE Transactions on Smart Grid*, 10(1):752–761, Jan 2019.

[13] M. Su, Z. Liu, Y. Sun, H. Han, and X. Hou. Stability analysis and stabilization methods of dc microgrid with multiple parallel-connected dc-dc converters loaded by cpls. *IEEE Transactions on Smart Grid*, 9(1):132–142, Jan 2018.

[14] C. Kammer and A. Karimi. Decentralized and distributed transient control for microgrids. *IEEE Transactions on Control Systems Technology*, pages 1–12, 2018.

[15] S. Cuk R. Middlebrook. Input filter considerations in design and application of switching regulators. *Proc. IEEE Ind. Appl. Annu. Meeting, Chicago, IL, USA*, 1976.

[16] C. M. Wildrick, F. C. Lee, B. H. Cho, and B. Choi. A method of defining the load impedance specification for a stable distributed power system. *IEEE Transactions on Power Electronics*, 10(3):280–285, May 1995.

[17] Jinjun Liu, Xiaogang Feng, F. C. Lee, and D. Borojevich. Stability margin monitoring for dc distributed power systems via perturbation approaches. *IEEE Transactions on Power Electronics*, 18(6):1254–1261, Nov 2003.

[18] Q.-C. Zhong and G. C. Konstantopoulos. Nonlinear current-limiting control for grid-tied inverters. In *2016 American Control Conference (ACC)*, pages 7472–7477, Boston, MA, USA, 6-8 July 2016.

[19] G. C. Konstantopoulos and Q. Zhong. Current-limiting dc/dc power converters. *IEEE Transactions on Control Systems Technology*, 27(2):855–863, March 2019.

[20] Z. J. Shen. Ultrafast solid-state circuit breakers: Protecting converter-based ac and dc microgrids against short circuit faults. *IEEE Electrification Magazine*, 4(2):72–70, June 2016.

[21] F. Duan, M. Xu, X. Yang, and Y. Yao. Canonical model and design methodology for LLC DC/DC converter with constant current operation capability under shorted load. *IEEE Trans. Power Electron.*, 31(10):6870–6883, Oct 2016.

[22] Y. Li, X. Mao, H. Wang, C. Wen, and L. Wen. An improved hiccup mode short-circuit protection technique with effective overshoot suppression for DC-DC converters. *IEEE Trans. Power Electron.*, 28(2):877–885, Feb 2013.

[23] Y. Li, X. Lai, Q. Ye, and B. Yuan. Novel short-circuit protection technique for DC-DC buck converters. *IET Circuits, Devices Systems*, 8(2):90–99, March 2014.

[24] A. Tilli and C. Conficoni. Control of shunt active filters with actuation and current limits. *IEEE Transactions on Control Systems Technology*, 24(2):644–653, March 2016.

[25] N. Bottrell and T. C. Green. Comparison of current-limiting strategies during fault ride-through of inverters to prevent latch-up and wind-up. *IEEE Trans. Power Electron.*, 29(7):3786–3797, 2014.

[26] A. C. Braitor, G. C. Konstantopoulos, and V. Kadirkamanathan. Power sharing of parallel operated DC-DC converters using current-limiting droop control. In *2017 25th Mediterranean Conference on Control and Automation (MED)*, pages 528–533, July 2017.

[27] A. P. N. Tahim, D. J. Pagano, E. Lenz, and V. Stramosk. Modeling and stability analysis of islanded dc microgrids under droop control. *IEEE Transactions on Power Electronics*, 30(8):4597–4607, Aug 2015.

[28] R. Ortega, Antonio Loria, Per Johan Nicklasson, and Hebertt Sira-Ramirez. *Passivity-based Control of Euler-Lagrange Systems, Mechanical, Electrical and Electromechanical Applications*. Springer-Verlag. Great Britain, 1998.

[29] J. W. Simpson-Porco, F. Dörfler, and F. Bullo. Voltage stabilization in microgrids via quadratic droop control. *IEEE Transactions on Automatic Control*, 62(3):1239–1253, March 2017.

[30] G. C. Konstantopoulos, Q. C. Zhong, B. Ren, and M. Krstic. Bounded integral control of input-to-state practically stable nonlinear systems to guarantee closed-loop stability. *IEEE Transactions on Automatic Control*, 61(12):4196–4202, Dec 2016.

[31] H.K.Khalil. *Nonlinear Systems*. Pearson, third edition, 2014.

[32] N. Pogaku, M. Prodanovic, and T. C. Green. Modeling, analysis and testing of autonomous operation of an inverter-based microgrid. *IEEE Transactions on Power Electronics*, 22(2):613–625, March 2007.